Ultrafast measurements of polarization switching dynamics on ferroelectric and anti-ferroelectric hafnium zirconium oxide

Mengwei Si (iD), Xiao Lyu, Pragya R. Shrestha, Xing Sun, Haiyan Wang (iD), Kin P. Cheung, and Peide D. Ye

View Online   Export Citation   CrossMark

ARTICLES YOU MAY BE INTERESTED IN

Ultrafast measurements of polarization switching dynamics on ferroelectric and anti-ferroelectric hafnium zirconium oxide

Mengwei Si,[1] Xiao Lyu,[1] Pragya R. Shrestha,[2,3] Xing Sun,[4] Haiyan Wang,[4] Kin P. Cheung,[3] and Peide D. Ye[1,a]

AFFILIATIONS

[1]School of Electrical and Computer Engineering and Birck Nanotechnology Center, Purdue University, West Lafayette, Indiana 47907, USA
[2]Theiss Research, La Jolla, California 92037, USA
[3]National Institute of Standards and Technology, Gaithersburg, Maryland 20899, USA
[4]School of Materials Science and Engineering, Purdue University, West Lafayette, Indiana 47907, USA

[a]Author to whom correspondence should be addressed: yep@purdue.edu

ABSTRACT

The ultrafast measurements of polarization switching dynamics on ferroelectric (FE) and antiferroelectric (AFE) hafnium zirconium oxide (HZO) are studied. The transient current during the polarization switching process is probed directly on the nanosecond scale. The switching time is determined to be as fast as 10 ns to reach fully switched polarization with characteristic switching times of 5.4 ns for FE HZO and 4.5 ns for AFE HZO by the nucleation limited switching model. The limitation by the parasitic effect on capacitor charging is found to be critical in the correct and accurate measurements of intrinsic polarization switching speed of HZO.

Published under license by AIP Publishing. https://doi.org/10.1063/1.5098786

Ferroelectric (FE) hafnium oxides (HfO$_2$), such as hafnium zirconium oxide (HZO), are promising thin film ferroelectric materials for nonvolatile memory applications, which feature fast speed,[1–9] long retention,[1,10] high endurance,[10–12] and a CMOS compatible fabrication process.[13,14] The time response of polarization switching is crucial to evaluate the potential operation speed of FE HfO$_2$ based ferroelectric devices, such as ferroelectric field-effect transistors (FeFETs)[1–3,15,16] and negative-capacitance field-effect transistors (NC-FETs).[17–20] However, the direct ultrafast measurement of transient polarization switching current in FE and antiferroelectric (AFE) HfO$_2$ metal-insulator-metal (MIM) capacitors on the single-digit nanosecond scale has not been reported previously. Meanwhile, the reported switching times of FE HfO$_2$ have a wide variety from a few ns to ms depending on different device structures and fabrication processes. Except for the well-known electric field dependence (faster at a higher electric field),[1,2] the reported polarization switching times at a high electric field still scatter from ∼10 ns to ∼1 μs,[1–9] which has not been clearly understood. Therefore, it is essential to directly probe and understand the polarization switching dynamics on the single-digit nanosecond scale and eventually down to the picosecond scale if the material intrinsically offers.

In this work, the transient polarization switching current is probed directly using an ultrafast pulse measurement setup. The polarization switching time is assumed to be as fast as 10 ns to reach fully switched polarization. The characteristic switching time is determined to be 5.4 ns for 15 nm thick FE HZO and 4.5 ns for 15 nm thick AFE HZO films by the nucleation limited switching (NLS) model. The time response is found to be mainly limited by the parasitic RC constant of the devices if a standard MIM capacitor with a large area is measured. As a result, thicker HZO (thickness between 4.5 nm and 15 nm) is found to switch faster partly due to a smaller capacitance involved.

HZO sandwiched by the tungsten nitride (WN) electrode capacitor structure is used for the ultrafast pulse measurements.[9] WN was deposited by atomic layer deposition (ALD) at 400 °C, using BTBMW (((CH$_3$)$_3$CN)$_2$ W(N(CH$_3$)$_2$)$_2$) and NH$_3$ as the W and N precursors. The ALD HZO (Hf:Zr = 1:1 for FE HZO and Hf:Zr = 1:3 for AFE HZO) film was deposited at 200 °C, using TDMAHf ([(CH$_3$)$_2$N]$_4$Hf), TDMAZr ([(CH$_3$)$_2$N]$_4$Zr), and H$_2$O as the Hf, Zr, and O precursors, respectively. The samples were annealed at 500 °C in a N$_2$ environment for 1 min by rapid thermal annealing. Figure 1(a) shows the cross-sectional transmission electron microscopy (TEM) and energy dispersive x-ray spectroscopy (EDS) images of the fabricated FE HZO
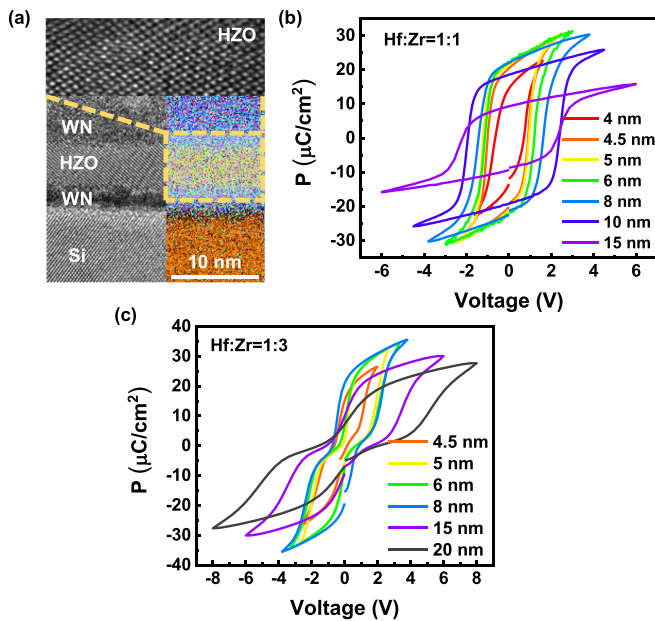
FIG. 1. (a) Cross-sectional TEM and EDS images of the fabricated FE HZO capacitor with WN electrodes, showing local crystalline HZO with the atomic resolution. (b) Polarization-voltage hysteresis loop of FE HZO capacitors with Hf:Zr = 1:1 at different thicknesses. (c) Polarization-voltage hysteresis loop of AFE HZO capacitors with Hf:Zr = 1:3 at different thicknesses.

capacitor, capturing the high quality and polycrystalline HZO. Figures 1(b) and 1(c) show the polarization-voltage (P-V) hysteresis loop of FE HZO and AFE HZO capacitors at different thicknesses.

Figure 2(a) shows the circuit diagram of the ultrafast measurement setup.[21] An ultrafast pulse generator, a variable gain transimpedance current amplifier, and an ultrafast high-definition oscilloscope were used for real-time monitoring of transient polarization switching current. The test circuit is carefully designed using an impedance-matched pickoff tee and is probed to minimize the signal reflection. The current amplifier was set at a trans-impedance gain of 100 V/A (maximum current 22 mA), corresponding to a bandwidth of 200 MHz and a rise time of 1.8 ns. A typical positive-up-negative-down (PUND) pulse sequence is used to distinguish the polarization switching current (I_{FE}) with the capacitor charging current in the measurement of FE HZO.[21] As shown in Fig. 2(b), a negative voltage pulse was used for the presetting of the polarization state. Then, two positive voltage pulses were applied to measure the polarization switching dynamics. The voltage pulses had a rising time (10% to 90%) of 2 ns and a pulse width of 1 μs to fully capture the polarization switching dynamics. The current in the first positive pulse (I_{pulse1}) is associated with the charging of the capacitor and the polarization switching together, while the current in the second positive pulse (I_{pulse2}) was the capacitor charging current only. Thus, the polarization switching current could be calculated as $I_{FE} = I_{pulse1} - I_{pulse2}$. For the measurement of the polarization switching in AFE HZO, a two-step presetting process was used. As shown in Fig. 2(c), a negative voltage pulse was used for the presetting of the polarization state, and then, an intermediate positive voltage pulse (for example, 2.5 V was used for 15 nm AFE HZO) was used to trigger one of the two polarization switching. Then,
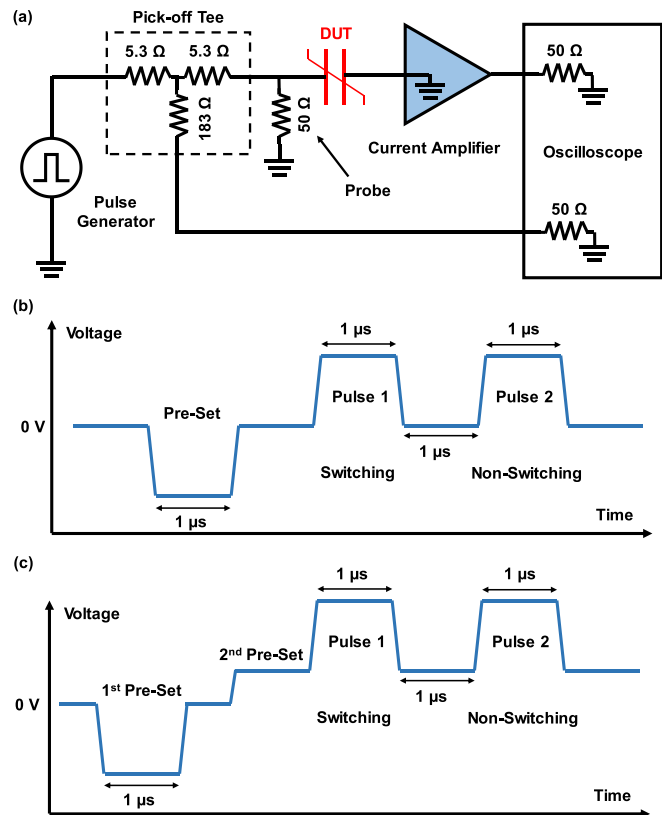

FIG. 2. (a) Circuit diagram of the ultrafast measurement setup. (b) The typical PUND pulse sequences for the FE measurement. (c) Pulse sequences for the AFE measurement.

two identical pulses were applied for the measurement of the other polarization switching.

Figures 3(a) and 3(b) show representative voltage and current measurement results of an 8 nm FE HZO capacitor with an area of 1960 μm^2. A slower switching example is chosen in Fig. 3(b) to better illustrate the difference between pulse 1 and pulse 2. As can be seen, I_{pulse1} is wider than I_{pulse2} due to the extra polarization switching current. Figure 3(c) shows the measurement of I_{pulse1}, I_{pulse2}, and I_{FE} on a 15 nm FE HZO capacitor with an area of 80 μm^2, showing the switching current response, nonswitching current response, and the calculated polarization switching current. The transient polarization charge density is calculated by integrating I_{FE} with respect to time, as $P = \int I_{FE}\,dt$, as shown in Fig. 3(d), where the applied voltage is 8.4 V and P/P_S is the normalized polarization (P_S is the saturation polarization). Note that the onset of polarization switching has a delay compared to the onset of the applied voltage pulse. One reason is the applied voltage pulse has a rise time of 2 ns. The other reason is that it also takes time for the HZO capacitor to be charged to a high enough voltage to trigger the polarization switching, as shown in the I_{pulse2} vs time characteristics, where only the capacitor charging process occurs. Therefore, t = 0 in Fig. 3(d) is determined when the polarization charge density starts to increase (apply to Fig. 3(f) similarly too). As can be seen clearly, a 10 ns fully saturated polarization switching is
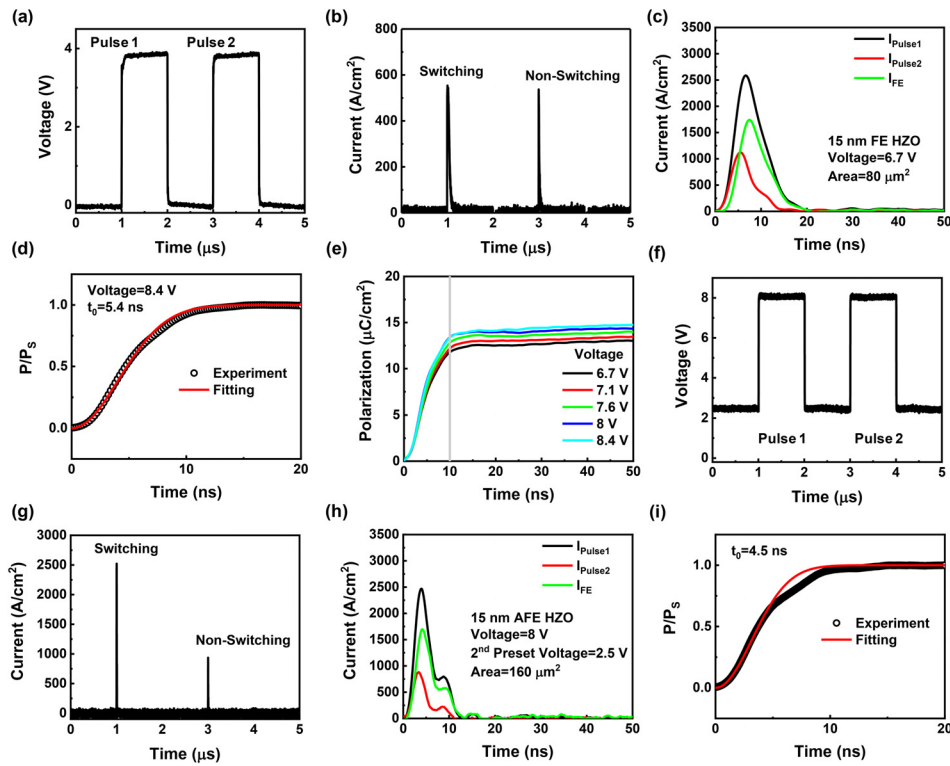
FIG. 3. Transient (a) voltage and (b) current characteristics on switching and nonswitching pulses of an 8 nm FE HZO capacitor with area = 1960 μm^2. (c) Transient current I_{pulse1}, I_{pulse2}, and I_{FE} of the 15 nm FE HZO capacitor. The device has an area of 80 μm^2. (d) Normalized polarization vs time characteristics by both the experiment and fitting by NLS model. A characteristic switching time of 5.4 ns is achieved. (e) Voltage-dependent polarization switching dynamics of the 15 nm FE HZO capacitor. Transient (f) voltage and (g) current characteristics on switching and nonswitching pulses of an 15 nm AFE HZO capacitor with the area = 160 μm^2. (h) Transient current I_{pulse1}, I_{pulse2}, and I_{FE} of the 15 nm AFE HZO capacitor. The device has an area of 160 μm^2. (i) Normalized polarization vs time characteristics by both experiment and fitting by the NLS model. A characteristic switching time of 4.5 ns is achieved.

achieved. To understand the switching dynamics and extract the characteristic switching time constant, the nucleation limited switching (NLS) model was applied for the multigrain polycrystalline HZO. In the NLS model, the polarization switching dynamics for a single elementary region is modeled as $P = P_S(1 - \exp(-(\frac{t}{t_0})^\beta))$, where β is an exponential parameter[7,22] and $\beta = 2$ is used in this work due to the best fitting and the 2-dimensional nature of the ultrathin FE film. t_0 is a voltage-dependent characteristic switching time. Note that the NLS model assumes a distribution of switching time, but for the simplicity of experimental extraction, a constant switching time is used. Figure 3(d) also shows comparison between the experimental P/P_S and NLS model. A characteristic switching time of $t_0 = 5.4$ ns is achieved for 15 nm thick FE HZO. Figure 3(e) shows the voltage-dependent characteristics of the polarization switching dynamics of 15 nm FE HZO at voltage from 6.7 V to 8.4 V. The switching speed difference is not clear except for a slight increase in the switched polarization charge density.

The measurement of transient polarization switching in AFE HZO is more complicated to distinguish the polarization switching current from capacitor charging current because in AFE materials, two polarization switching events occur when the applying voltage sweeps from negative to positive. The two-step presetting process in Fig. 2(c) is used so that pulse 1 triggers the polarization switching, while during pulse 2, only capacitor charging occurs. Figures 3(f) and 3(g) show representative voltage and current measurement results of an 15 nm FE HZO capacitor with an area of 160 μm^2. The voltage in the first presetting pulse, pulse 1, and pulse 2 is 8 V in absolute value. 2.5 V is used for the second preset, as shown in Fig. 3(f). Figure 3(h) shows the measurements of I_{pulse1}, I_{pulse2}, and I_{FE} of a 15 nm AFE HZO capacitor

with an area of 160 μm^2, extracted from the same measurement as in Figs. 3(f) and 3(g). Figure 3(i) shows the corresponding normalized polarization vs time characteristics of the experimental data and fitting by the NLS model. A characteristic switching time of $t_0 = 4.5$ ns is achieved for 15 nm thick AFE HZO. From the switching current [Figs. 3(c) and 3(h)] and the transient polarization charge density [Figs. 3(d) and 3(i)], it is found that the switching speed of AFE HZO is faster than that of FE HZO with the same thickness. The little bumps in the transient switching current [Figs. 3(c) and 3(h)] are due to signal reflections. Since signal reflections are nonideal, the experimental data deviate slightly from the NLS model where the reflections occur.

As can be seen from Fig. 3, the polarization switching needs sufficient charges from the current flow. Thus, the speed of this process could be limited by the RC constant of the devices beyond the intrinsic switching speed of FE or AFE films. As the polarization switching current can be much higher than the capacitor charging current, the RC effect can have a more severe impact on the measurement of polarization switching than capacitor charging. It is important to make sure that the experiments measure the intrinsic polarization switching dynamics instead of the RC time constant of the device. One way to exclude the impact of the RC effect is to use a small capacitor area and highly conductive metal as electrodes so that the RC time constant becomes sufficiently small. Figure 4(a) shows the measurements of I_{FE} on 15 nm FE HZO with capacitor areas from 25 μm^2 to 17 700 μm^2. It is found that polarization switching current (normalized by the area) becomes significantly smaller and the I_{FE} peak appears later in larger area capacitors. The polarization vs time characteristics are shown in Figs. 4(b) and 4(c). These results indicate that the I_{FE} measurements in large areas are limited by the RC effect and cannot reflect the intrinsic
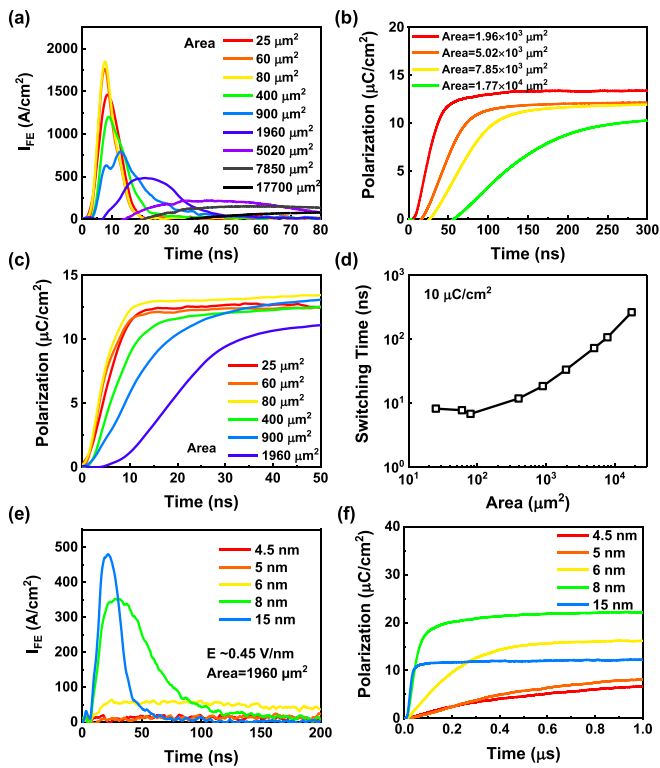
FIG. 4. Transient polarization switching current of the 15 nm FE HZO capacitor at different areas. (b) and (c) The corresponding polarization vs time characteristics of (a). (d) Ferroelectric switching time (from 0 to 10 μC/cm^2) at different areas. (e) Transient polarization switching current of the FE HZO capacitor at different thicknesses. The electric field applied is $\sim$0.45 V/nm, and the areas of measured devices are 1960 μm^2. (f) The corresponding polarization vs time characteristics of (e).

polarization switching speed of HZO. Figure 4(d) shows the polarization switching time (defined by polarization charge density reaching 10 μC/cm^2) vs the capacitor area, showing that the switching time saturates when the area is below about a few hundred μm^2. The saturation of switching time in the small area limit indicates that the RC effect is almost eliminated. A switching time of 6.9 ns (polarization from 0 to 10 μC/cm^2) is achieved for a 15 nm FE HZO film. These results also suggest the necessity of studying the capacitor area dependence when reporting the switching speed of ferroelectric materials. Note that similar switching time saturation is observed in AFE HZO and the characteristic switching time of AFE HZO presented in Fig. 3 is not affected by the RC constant either. Figure 4(e) shows the I_{FE} vs time characteristics of FE HZO capacitors with the thickness from 4.5 to 15 nm and a fixed area of 1960 μm^2. The electric field is controlled to be around 0.45 V/nm with different thicknesses and applied voltages. Figure 4(f) shows the corresponding transient polarization charge density. The thinner HZO capacitors have a larger polarization switching time, partly because the capacitors with thinner HZO have a larger capacitance, which can also slow down the charge balance process. Note that a significant difference is observed between the speed of the thin FE HZO film and thick FE HZO film. For example, the 15 nm HZO film becomes fully polarized in less than 100 ns, while the 4.5 nm or 5 nm HZO films need more than 1 μs to reach full

polarization switching. The speed difference is larger than the expectation from the RC time constant only. Other factors, such as the grain size, thickness-dependent coercive electric fields,[9] and intrinsic thickness-dependent switching speed, may play an important role in the FE HZO polarization switching dynamics.

In summary, ultrafast measurements of transient polarization switching processes on FE and AFE HZO films are studied. Except for the extremely fast measurement setup, the experiments are also carefully designed to exclude the impact of the RC effect from the measured devices. The switching time is achieved to be as fast as single-digit nanoseconds for FE and AFE HZO films supported by the multigrain NLS model.

REFERENCES

[1] J. Müller, T. S. Böscke, U. Schröder, R. Hoffmann, T. Mikolajick, and L. Frey, IEEE Electron Device Lett. **33**, 185 (2012).

[2] E. Yurchuk, J. Müller, J. Paul, T. Schlösser, D. Martin, R. Hoffmann, S. Müeller, S. Slesazeck, U. S. Member, R. Boschke, R. Van Bentum, T. Mikolajick, U. Schröder, R. Boschke, R. Van Bentum, and T. Mikolajick, IEEE Trans. Electron Devices **61**, 3699 (2014).

[3] H. K. Yoo, J. S. Kim, Z. Zhu, Y. S. Choi, A. Yoon, M. R. MacDonald, X. Lei, T. Y. Lee, D. Lee, S. C. Chae, J. Park, D. Hemker, J. G. Langan, Y. Nishi, and S. J. Hong, in Proceedings of the IEEE International Electron Devices Meeting (2017), pp. 481–484.

[4] H. Mulaosmanovic, J. Ocker, S. Müller, U. Schroeder, J. Müller, P. Polakowski, S. Flachowsky, R. Van Bentum, T. Mikolajick, and S. Slesazeck, ACS Appl. Mater. Interfaces **9**, 3792 (2017).

[5] S. Dünkel, M. Trentzsch, R. Richter, P. Moll, C. Fuchs, O. Gehring, M. Majer, S. Wittek, B. Müller, T. Melde, H. Mulaosmanovic, S. Slesazeck, S. Müller, J. Ocker, M. Noack, D. A. Löhr, P. Polakowski, J. Müller, T. Mikolajick, J. Höntschel, B. Rice, J. Pellerin, and S. Beyer, in Proceedings of the IEEE International Electron Devices Meeting (2017), pp. 485–488.

[6] W. Chung, M. Si, P. R. Shrestha, J. P. Campbell, K. P. Cheung, and P. D. Ye, in Proceedings of Symposium on VLSI Technology (2018), pp. T89–T90.

[7] C. Alessandri, P. Pandey, A. Abusleme, and A. Seabaugh, IEEE Electron Device Lett. **39**, 1780 (2018).

[8] Z. Zheng, R. Cheng, Y. Qu, X. Yu, W. Liu, Z. Chen, B. Chen, Q. Sun, D. W. Zhang, and Y. Zhao, IEEE Electron Device Lett. **39**, 1469 (2018).

[9] X. Lyu, M. Si, X. Sun, M. A. Capano, H. Wang, and P. D. Ye, in Proceedings of Symposium on VLSI Technology (2019).

[10] N. Gong and T. P. Ma, IEEE Electron Device Lett. **37**, 1123 (2016).

[11] Y. C. Chiu, C. H. Cheng, C. Y. Chang, M. H. Lee, H. H. Hsu, and S. S. Yen, in Proceedings of Symposium on VLSI Technology (2015), pp. T184–T185.

[12] K. Ni, P. Sharma, J. Zhang, M. Jerry, J. A. Smith, K. Tapily, R. Clark, S. Mahapatra, and S. Datta, IEEE Trans. Electron Devices **65**, 2461 (2018).

[13] T. S. Böscke, J. Müller, D. Bräuhaus, U. Schröder, and U. Böttger, Appl. Phys. Lett. **99**, 102903 (2011).

[14] J. Müller, T. S. Böscke, U. Schröder, S. Mueller, U. Böttger, L. Frey, and T. Mikolajick, Nano Lett. **12**, 4318 (2012).

[15] H. Ishiwara, J. Nanosci. Nanotechnol. **12**, 7619 (2012).

[16] M. Si, P.-Y. Liao, G. Qiu, Y. Duan, and P. D. Ye, ACS Nano **12**, 6700 (2018).

[17] S. Salahuddin and S. Datta, Nano Lett. **8**, 405 (2008).

[18] K.-S. Li, P.-G. Chen, T.-Y. Lai, C.-H. Lin, C.-C. Cheng, C.-C. Chen, Y.-J. Wei, Y.-F. Hou, M.-H. Liao, M.-H. Lee, M.-C. Chen, J.-M. Sheih, W.-K. Yeh, F.-L.

Yang, S. Salahuddin, and C. Hu, in *Proceedings of the IEEE International Electron Devices Meeting* (2015), pp. 620–623.

[19]Z. Krivokapic, U. Rana, R. Galatage, A. Razavieh, A. Aziz, J. Liu, J. Shi, H. J. Kim, R. Sporer, C. Serrao, A. Busquet, P. Polakowski, J. Müller, W. Kleemeier, A. Jacob, D. Brown, A. Knorr, R. Carter, and S. Banna, in *Proceedings of the IEEE International Electron Devices Meeting* (2017), pp. 357–340.

[20]M. Si, C.-J. Su, C. Jiang, N. J. Conrad, H. Zhou, K. D. Maize, G. Qiu, C.-T. Wu, A. Shakouri, M. A. Alam, and P. D. Ye, Nat. Nanotechnol. **13**, 24 (2018).

[21]A. Grigoriev, M. M. Azad, and J. McCampbell, Rev. Sci. Instrum. **82**, 124704 (2011).

[22]J. Y. Jo, H. S. Han, J. G. Yoon, T. K. Song, S. H. Kim, and T. W. Noh, Phys. Rev. Lett. **99**, 267602 (2007).